Packing structure of semiflexible rings

Leopoldo R. Gómez[a,1,2], **Nicolás A. García**[b,1], and **Thorsten Pöschel**[c]

[a]Department of Physics, Universidad Nacional del Sur-IFISUR-CONICET, 8000 Bahía Blanca, Argentina; [b]Theory Group, Institut Laue-Langevin, 38042 Grenoble, France; and [c]Institut für Multiscale Simulation, Friedrich-Alexander-Universität Erlangen-Nürnberg, 91052 Erlangen, Germany

Unraveling the packing structure of dense assemblies of semiflexible rings is not only fundamental for the dynamical description of polymer rings, but also key to understand biopackaging, such as observed in circular DNA of viruses or genome folding. Here we use X-ray tomography to study the geometrical and topological features of disordered packings of rubber bands in a cylindrical container. Assemblies of short bands assume a liquid-like disordered structure, with short-range orientational order, and reveal only minor influence of the container. In the case of longer bands, the confinement causes folded configurations and the bands interpenetrate and entangle. Most of the systems are found to display a threading network which percolates the system. Surprisingly, for long bands whose diameter is more than twice the diameter of the container, we found that all bands interpenetrate each other, in a complex fully entangled structure.

filamentous matter | entanglements | X-ray tomography | geometry | topology

The structural and dynamical properties of melts of noncon-catenated circular polymers stand as one of the most controversial and interesting topics in polymer physics (1, 2). Here, the reptation (end-directed curvilinear diffusion) of chains, as occurs in linear or ramified polymers (3), is inhibited because of the absence of free ends in the ring molecules. Therefore the conformations, relaxation, and diffusion mechanisms of systems of rings remain unclear.

Due to the topological constraints of nearby rings, early models of the dynamics of polymer rings assume that the molecules in melts adopt lattice animal configurations, where each bond in the animal represents a doubled polymer strand (1, 4–6). Neglecting mutual threading of the rings, the chains are assumed to relax stress by sliding along the contour of other loops, which leads to a power-law relaxation, in agreement with experiments (7). Simulations of ideally flexible polymer rings showed, however, that the molecules form more compact crumpled globules (8–10), and there can be strong intercoil interactions (11–13), which slow down the dynamics of the system, even to glass-like behavior (2, 14, 15).

Despite the progress in understanding systems of fully flexible rings, much less is known on the structural properties for the case of semiflexible polymer rings. Here, a good comprehension of the fundamental features of dense packings of semiflexible rings should be also essential for understanding biopackaging (16, 17), such as observed in circular DNA of bacteriophage viruses or prokaryote and eukaryote cells. For these biological systems, the compliance of efficient packing and their functionality in the process of genomic reproduction remains yet unclear.

Here we study disordered assemblies of rubber bands which represent rather systems which reveal the property of entanglement. Despite being athermal, these simple systems display the key features observed in circular filamentous matter and, as shown below, allow the detailed characterization of topology and entanglements as functions of the band's length.

The disordered, entangled systems studied here are obtained by placing the bands one by one in a cylindrical container of radius $R_c = 3.25$ cm and height 7.2 cm and subsequent mixing by mechanical agitation. The structural properties of the packings are obtained by means of X-ray tomography and subsequent data analysis to locate each band individually (see *SI Appendix* for details on sample preparation and segmentation analysis).

Fig. 1 shows typical packings of rubber bands of different lengths as obtained from the tomograms. Movies S1–S3 show further examples of the raw X-ray data, assembly reconstruction, and individual chain configurations. Having identified all bands of the system, we study the geometrical and topological features of these entangled structures (18).

Obviously, the lengths of the bands must influence the packing structure, and this is the effect we study here. To this end, we characterize packings of bands of different lengths at similar packing fractions, $\phi \sim 0.17$. Table 1 summarizes the main characteristics of types of bands used. These are the persistence length, L_p, characterizing the stiffness of the rings, and the number of rings, N_{rings}, used to obtain similar packing fractions, ϕ. Finally, the aspect ratio between the radius of gyration of the rings and the radius of the cylinder, R_g/R_c, quantifies the degree of confinement, specified below.

To check for robustness of our results, for each type, A to E, we prepared three packings independently. The subsequent analysis did not reveal significant differences in both geometrical and topological features. For details see *SI Appendix*.

Significance

Understanding the structure of disordered assemblies of ring molecules is key for the description of polymer rings and cyclic biomolecules. Here we study the geometrical and topological properties of these systems by imaging disordered assemblies of macroscopic rubber bands through X-ray tomography. Commonly, these systems contain networks of interthreading bands which percolate the whole assembly. But when the bands are much longer than the container, we observe the formation of fully entangled states, where each band is in the neighborhood of the others. Thus, confined semiflexible ring macromolecules are expected to have extremely correlated configurations with very slow glassy-like dynamics.

Fig. 1. Packing structure of confined rubber bands. Shown are X-ray tomograms of bands' packing of different lengths. From *Left* to *Right* the tomograms correspond to bands of types A, B, C, and E (Table 1).

Geometrical Properties

Fig. 2 *A–C* shows typical reconstructions for bands' packings of different lengths. In Fig. 2 *A–C*, *Top* different bands are displayed by different colors, and in Fig. 2 *A–C*, *Bottom* one of the bands is highlighted to provide a visual impression of the structure. A more quantitative characteristic is the shape tensor (19),

$$Q_{ij} = \frac{1}{L}\int \mathbf{r}_i(s)\mathbf{r}_j(s)\,\mathrm{d}s - \frac{1}{L^2}\int \mathbf{r}_i(s)\,\mathrm{d}s\int \mathbf{r}_j(s)\,\mathrm{d}s, \quad [1]$$

averaged over the bands in the sample.

The invariants of this tensor, which characterize the geometry of the rings, are the radius of gyration given by the trace of the shape operator, $R_g^2 = \mathrm{Tr}\,Q$; the asphericity $\Delta = \frac{3\,\mathrm{Tr}\,\tilde{Q}^2}{2(\mathrm{Tr}\,\tilde{Q})^2}$; and the nature of the asphericity $\Sigma = 4\det\tilde{Q}/(2/3\,\mathrm{Tr}\,\tilde{Q}^2)^{3/2}$, where $\tilde{Q}_{ij} = Q_{ij} - \delta_{ij}\,\mathrm{Tr}\,Q/3$. The asphericity assumes values $0 \leq \Delta \leq 1$, where the limits $\Delta = 0$ represent a fully symmetric object and $\Delta = 1$ a fully extended rod-like object. The nature of asphericity assumes values $-1 \leq \Sigma \leq 1$. Here $\Sigma = -1$ represents an oblate object, and $\Sigma = 1$ for a prolate object.

Fig. 2*D* shows the values of Δ and Σ, obtained for the ensembles of rings of different length (the distributions of Δ and Σ for different bands are provided in *SI Appendix*). For the shortest bands (Fig. 2*A*) we found $\Sigma \approx -1$ and $\Delta \approx 0.3$, showing that most bands pack like planar nearly undistorted circular rings (for a rigid ring we would find $\Sigma = -1$ and $\Delta = 0.25$).

For longer bands, we observe that the bands fold due to the confinement by the container (Fig. 2 *B* and *C*). First, some bands start to fold into "eight"-like configurations (Fig. 2*B*). For yet longer bands the confinement enforces more complex folding patterns (Fig. 2*C*). The averaged shape invariants show that Δ decreases toward 0 and Σ remains positive for long bands. This means that with increasing length the bands acquire more symmetric configurations, with an average prolate form. This asymptotic prolate shape is a direct consequence of the cylindrical container (confinement effect).

The third shape invariant is the radius of gyration of the bands. For polymer rings, it is found that the average-square gyration radius scales with a power law with the total contour length $R_g^2 \sim L^{2\nu}$, where the characteristic exponent varies from model to model: $\nu = 1/2$ for rings folded into linear ribbons, $\nu = 1/4$ for ideal lattice trees or animals (1), and $\nu = 1/3$ for rings with the shape of crumpled globules (10). Fig. 2 *D*, *Inset* shows the average radius of gyration squared as a function of bands' lengths. Here, for long bands we found an exponent near $\nu = 1/4$ (red line). However, a visual inspection in Fig. 2 *B* and *C* reveals that ring configurations clearly differ from lattice trees or animals, mostly due to ring

semiflexibility and threading. This is also different from the crumpled globules observed in simulations of fully flexible polymer rings (8–10). Table 1 shows that indeed the degree of confinement is high ($R_g/R_c \approx 0.9$) for the longest bands.

The geometrical properties of the bands can be further studied through the Frenet–Serret expressions (20, 21)

$$\frac{d\mathbf{T}}{ds} = \kappa\mathbf{N}$$
$$\frac{d\mathbf{N}}{ds} = -\kappa\mathbf{T} + \tau\mathbf{B}$$
$$\frac{d\mathbf{B}}{ds} = -\tau\mathbf{N}, \quad [2]$$

where s is the arc length, and $\mathbf{T}$, $\mathbf{N}$, and $\mathbf{B}$ are the local tangent, normal, and binormal vectors, respectively (Fig. 2*E*). The values of κ and τ represent the local curvature and torsion of bands.

Due to short bands behaving as nearly undistorted planar rings, an average band orientation can be obtained by averaging the binormals (Fig. 2 *F*, *Inset*). Then, orientational correlations between near bands can be quantified through the order parameter $S(r) = \langle\frac{3}{2}\cos^2\theta(r) - 1\rangle$, where $\theta(r)$ is the misorientaton between bands' binormals separated by a distance r, and the average is performed over the entire system. Fig. 2*F* shows that at short distances (of the order of the band's radius r_0) the binormals are somewhat aligned, such that short bands pack parallel to their near neighbors, depicting short-range orientational correlations (blue line). This local discotic order was also observed in simulations of short polymer rings (22) and is a consequence of excluded volume interactions. For longer bands, this short-range order disappears due to chain flexibility (red line in Fig. 2*F*).

Let us consider the distribution of the local curvature, $P(\kappa)$, of the bands. Fig. 2*G* shows $P(\kappa)$ for the shortest bands (black line dots) and for the rest of the bands (colored lines), where the curvature κ is normalized by the peak κ_{peak} value of the curvature distribution. We found that κ_{peak} decays with a power law with the bands' length $\kappa_{\text{peak}} \sim L^{-1/2}$ (*SI Appendix*, Fig. S7). Fig. 2*G*

Table 1. Rubber band's main properties

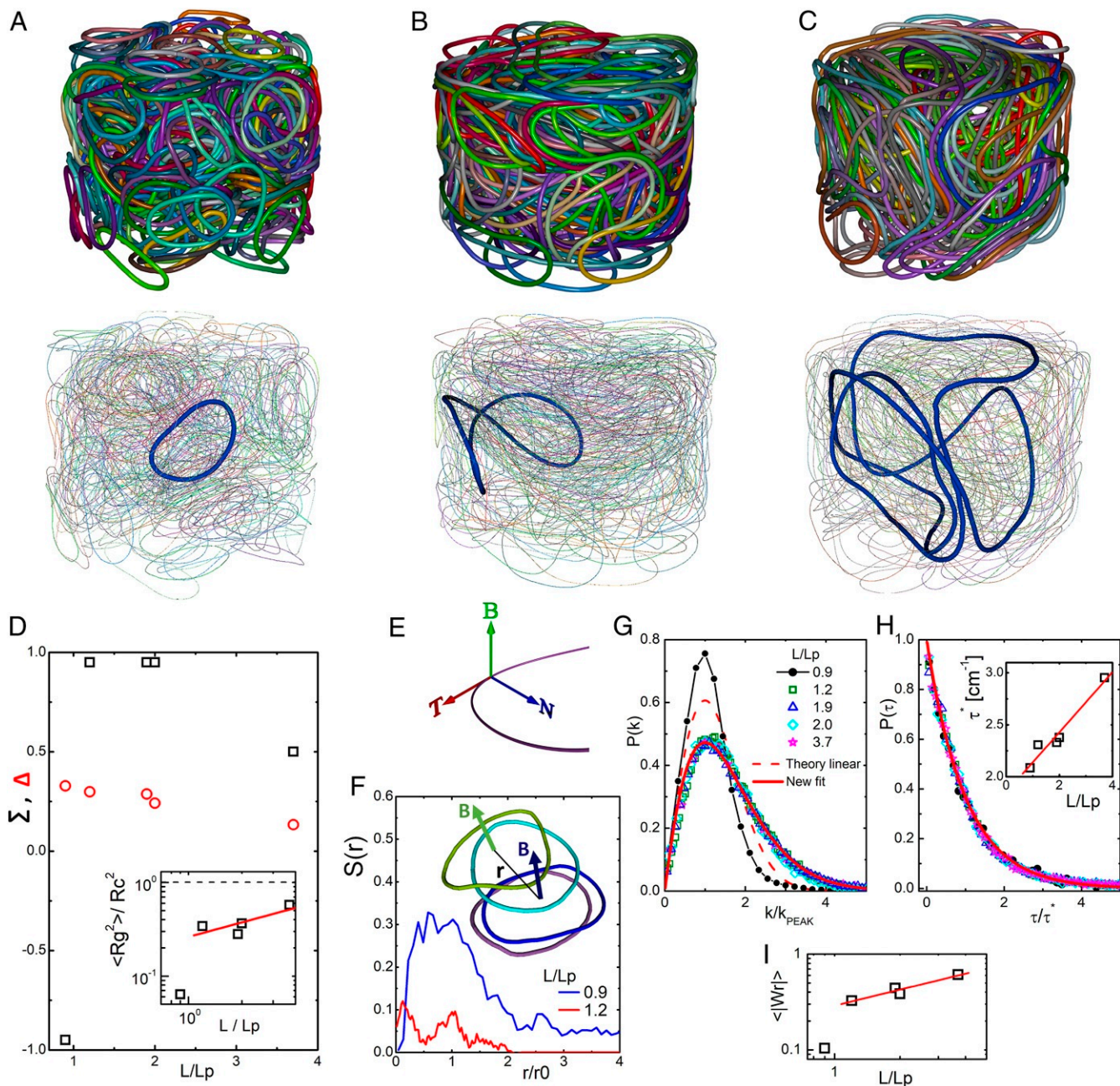| type	L (cm)	L/Lp	N_{rings}	ϕ	R_g/R_c
A	7.6	0.9	331	0.145	0.35
B	20.4	1.2	130	0.159	0.68
C	24.1	1.9	71	0.172	0.61
D	30.4	2.0	58	0.186	0.70
E	63.4	3.7	28	0.180	0.87

Fig. 2. Geometrical analysis of bands. (*A*–*C*, *Top*) Typical reconstruction of packings, where the different rubber bands can be distinguished by color. (*A*–*C*, *Bottom*) A single band is highlighted in blue color while the others appear thinner to improve visibility. (*D*) Averaged shape invariants Σ and Δ as functions of the bands' lengths. *Inset* shows the squared radius of gyration, the red line is a power-law fit for long chains, and the dashed line illustrates the ceiling $R_g^2 = R_c^2$. (*E*) Scheme of the Frenet–Serret frame. (*F*) Orientational correlations as a function of length *r*, normalized with the radius of bands r_0. (*G*) Curvature distribution of bands. The dashed red line shows the theoretical prediction for the curvature distribution of linear semiflexible polymers, and the solid red line shows a fit. (*H*) Torsion distribution of bands. The solid red line is a single exponential. *Inset* shows the dependence of τ^* with length. (*I*) Average writhe of bands as a function of length.

shows that the curvature distribution for long bands nicely collapses on a master curve. On the contrary, the distribution for the shortest (almost undistorted) rings clearly displays a different, more narrowed, curvature distribution. Note that for very rigid rings ($L_p >> L$) there should be small distortions from a circular shape, and the curvature distribution is expected to became a Gaussian centered in the intrinsic curvature $\kappa_0 = 1/r_0$, with r_0 the radius of rings.

For comparison, in Fig. 2*G* we also include the prediction for the curvature distribution of linear semiflexible polymers

(dashed red line), which is of the form $P(\widetilde{k}) = \widetilde{\kappa} \exp(-\widetilde{\kappa}^2/2)$, $\widetilde{\kappa} = \kappa/\kappa_{peak}$ (23–25). In contrast to linear semiflexible polymers, the rubber bands studied here display a wider distribution of the curvature, such that the probability of finding regions of large values of curvature is higher, as it can be expected due to the cyclic topology of chains. Here we found that the curvature of long bands can be well approximated by the expression $P(\widetilde{k}) = \widetilde{\kappa} \exp(-3 \widetilde{\kappa}^{4/3}/4)$, corresponding to a generalized Gamma distribution (shown as a solid red line in Fig. 2*G*).
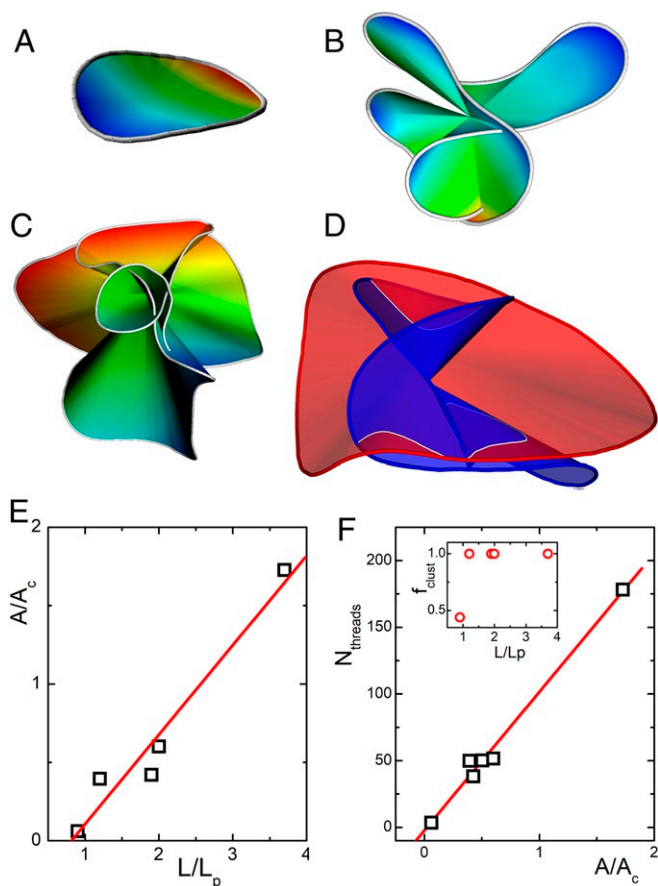
Fig. 3. Threading analysis. (*A*–*C*) Examples of minimal surfaces obtained for bands of different lengths. (*D*) Twice threading of one band (in blue) over another (red). (*E*) Averaged area A of the minimal surfaces, normalized with the section of the container A_c, as a function of the band's length. The line represents a linear fit. (*F*) Averaged number of threading on bands as a function of the area of the minimal surfaces A. *Inset* shows the size of the largest interthreading cluster as a function of length. Note that only for the shortest bands (system A) the threading cluster does not percolate the system.

In Fig. 2*H* we show the distribution of the absolute value of torsion of bands $P(\tau)$, for all of the system studied. In this plot the torsion of the bands is normalized with a characteristic torsion τ^*, which scales linearly with the band's length (Fig. 2 *H*, *Inset*). Clearly, when normalizing with τ^*, the torsion distribution of all of the systems collapses in a universal master curve, which can be well approximated by a single exponential decay function (red line in Fig. 2 *H*, *Inset*) $P(\widetilde{\tau}) = \exp(-\widetilde{\tau})$, with $\widetilde{\tau} = \tau/\tau^*$.

The folding of bands can also be quantified through the writhe W_r, which measures the degree of coiling of a closed curve, by counting the number of crossings of the curve with its axis (26),

$$W_r = \frac{1}{4\pi} \oint \oint \frac{(d\mathbf{r}_1 \times d\mathbf{r}_2)\mathbf{r}_{12}}{|\mathbf{r}_{12}|^3}, \qquad [3]$$

where $\mathbf{r}_1$ and $\mathbf{r}_2$ are the points along the curve, and $\mathbf{r}_{12} = \mathbf{r}_2 - \mathbf{r}_1$. The writhe has been mainly used to characterize the supercoiling transition of circular DNA (27, 28), but also to distinguish configurations obtained in simulations of flexible and semiflexible polymers, in bulk and under confinement (29, 30). For polymers in bulk, it has been found that $\langle |W_r| \rangle \sim L^{1/2}$ and the exponent of the scaling increases in the case of confinement. Fig. 2*I* shows that for our confined semiflexible bands

the average writhe scales with the contour length with a similar exponent $\langle |W_r| \rangle \sim L^{0.55}$. It has been argued that for closed curves in space, the absolute value of writhe cannot grow faster than $\langle |W_r| \rangle \sim L^{4/3}$, where the $4/3$ is an upper bound for the exponent (26).

Topological Properties

Threading Number and Network. Up to now, we have focused on the averaged geometrical properties of bands. The confinement does, however, cause not only folding of the bands, but also entanglement and mutual interpenetration. For long bands we can expect a highly entangled structure, which is considered in this section.

The bands' threading can be studied through a minimal surface analysis. This technique was proposed to study threading in simulations of fully flexible polymer rings (12, 13). The idea is that the minimal surface spanned by a ring's contour (Fig. 3 *A*–*C*) can be used to estimate the number of topological conflicts among overlapping rings through the intersection of the minimal surfaces (Fig. 3*D*). Fig. 3*E* shows that the area of the minimal surfaces linearly scales with the length of bands.

In Fig. 3*F* we show the average total number of threadings on a band, as a function of the minimal surface area. Note that the total number of threadings on a ring can be much larger than the number of rings due to multiple threadings (which is rather common for long bands). Here we find that the number of threadings increases linearly with the area expanded by the band's contour (red line in Fig. 3*E*). As the length of rings increases (at similar packing fractions) there is a corresponding increase in the number of threadings. Clearly, the larger the area the band expands, the more probable it will be threaded by other bands.

It is expected that a network of interthreading rings will naturally emerge in these highly entangled systems. Such a network,
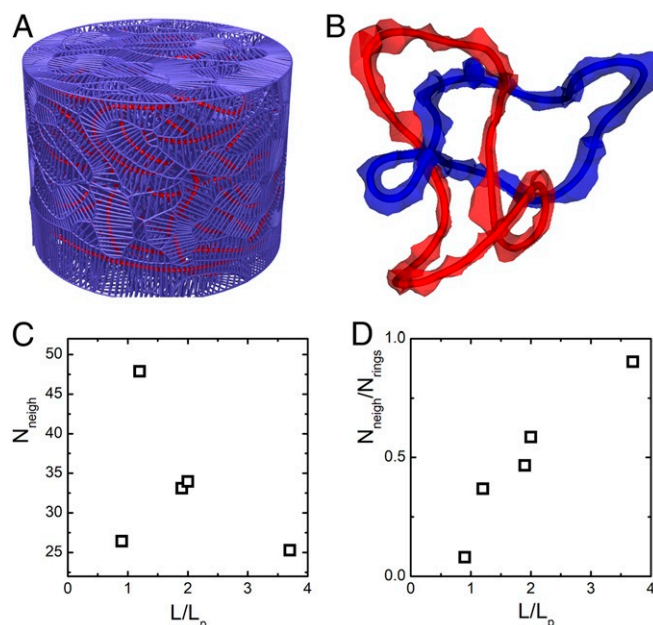

Fig. 4. Voronoi analysis. (*A*) Voronoi partition of space by using the particles of all chains in the system. (*B*) Voronoi tubes defining the closest regions on the red and blue bands (the rest of the bands in the packing are not shown). (*C*) Average number of neighbors on bands as a function of length. (*D*) The fraction of the system which is neighbors of a band, as a function of length. Note that for the longest bands, all of the bands are first neighbors, resulting in a fully entangled structure.

depending on its size, will probably slow down the dynamics of thermal systems (2, 15). Here, to characterize such threading networks in our system, in Fig. 3 *F*, *Inset* we plot the size of the larger cluster of interthreading rings, normalized by the number of rings in the structure $f_{\text{clust}} = N_{\text{clust}}/N_{\text{rings}}$, as a function of the length of bands. Note that we find a percolating network of threading bands for most of the systems studied. Only the shortest bands (system A) do not establish a threading network spanning the entire system, but the larger cluster involves only half the system approximately.

Generalized Voronoi Diagrams. Note, however, that the interpenetration of bands gives only partial information on the entanglements and topology of the structure. Many rings in the packings are very close, however, not interpenetrating. These not-interpenetrating rings should also influence the static properties of disordered packings and the dynamical response of thermal systems like ring polymer melts or confined circular DNA.

To complete the characterization of the rings' environment, we introduce a Voronoi partition of space by using the particles of all chains in our systems, as if they were unlinked (Fig. 4*A*). Next, we merge all of the Voronoi volumes corresponding to particles belonging to the same chain. This process produces a Voronoi tessellation, where all of the bands are contained in their closest tubular-like region (Fig. 4*B*). With this tessellation we can obtain the number of bands which are first neighbors of each band (coordination number). Fig. 4*C* shows the averaged coordination number as a function of the band's length. The distributions of neighbors per band can be observed in *SI Appendix,* Fig. S8.

Even for the smallest bands we find a coordination number of 26, which approximately doubles the coordination of dense liquids and solids. In our case, the maximum coordination number is achieved by system B, with about 50 band's neighbors. For the largest bands the coordination number decreases, but this is just because the number of bands in the packing decreases. Fig. 4*D* shows the coordination number normalized with the number of bands in the structure, as a function of length. This fractional coordination number grows monotonously with the bands' length, showing that the system gets more entangled for longer bands. Remarkably, for the longest bands, it is observed that all of the bands are first

neighbors of each other, forming a complex disordered fully entangled structure. It is expected that thermal systems with a similar degree of entanglement will display extremely slow dynamics.

It is interesting to compare the results obtained here for the topology of the structure of semiflexible filamentous matter with previous ideas and results concerning melts of fully flexible rings. It is clear that the configurations of the semiflexible rings are far from lattice animals or crumpled globules, where interthreading should be marginal, as obtained for fully flexible molecules. Here, the semiflexibility of rings produces more open configurations, favoring interthreading and entanglements. This is not too surprising because, even for linear molecules, the stiffness of molecules induces more expanded configurations and more entanglements (31). Our structural analysis suggests that, contrary to fully flexible rings, semiflexible rings should have much slower dynamics than their linear counterparts. We hope this work can motivate further studies on the dynamics of semiflexible polymer rings and circular biomolecules.

Conclusion. Since Bernal's early contributions, the in-depth analyses of the close-packed structures made of spheres (32), ellipsoids (33), tetrahedra (34), other compact objects (35), and granular chains (36) have improved our current vision of crystals, liquids, and glasses. Such studies have revealed that molecular geometry and symmetry, independent of the specific microscopic details and interactions, stand at the end of the structure of condensed matter. In the same line, here we have shown that a simple bunch of rubber bands can be used to elucidate the universal structural features of disordered filamentous matter, which should be key in the description of synthetic polymers and biomolecules, among others.

1. M. Rubinstein, Dynamics of ring polymers in the presence of fixed obstacles. *Phys. Rev. Lett.* **57**, 3023–3026 (1986).
2. E. Lee, S. Kim, Y. J. Jung, Slowing down of ring polymer diffusion caused by inter-ring threading. *Macromol. Rapid Commun.* **36**, 1115–1121 (2015).
3. M. Rubinstein, R. H. Colby, *Polymer Physics* (Oxford University Press, New York, NY, 2003), vol. 23.
4. S. P. Obukhov, M. Rubinstein, T. Duke, Dynamics of a ring polymer in a gel. *Phys. Rev. Lett.* **73**, 1263–1266 (1994).
5. S. T. Milner, J. D. Newhall, Stress relaxation in entangled melts of unlinked ring polymers. *Phys. Rev. Lett.* **105**, 208302 (2010).
6. A. Y. Grosberg, Annealed lattice animal model and Flory theory for the melt of non-concatenated rings: Towards the physics of crumpling. *Soft Matter* **10**, 560–565 (2014).
7. M. Kapnistos *et al.*, Unexpected power-law stress relaxation of entangled ring polymers. *Nat. Mater.* **7**, 997 (2008).
8. T. Vettorel, A. Y. Grosberg, K. Kremer, Statistics of polymer rings in the melt: A numerical simulation study. *Phys. Biol.* **6**, 025013 (2009).
9. J. D. Halverson, W. B. Lee, G. S. Grest, A. Y. Grosberg, K. Kremer, Molecular dynamics simulation study of nonconcatenated ring polymers in a melt. I. Statics. *J. Chem. Phys.* **134**, 204904 (2011).
10. A. Rosa, R. Everaers, Ring polymers in the melt state: The physics of crumpling. *Phys. Rev. Lett.* **112**, 118302 (2014).
11. D. Michieletto, D. Marenduzzo, E. Orlandini, G. P. Alexander, M. S. Turner, Threading dynamics of ring polymers in a gel. *ACS Macro Lett.* **3**, 255–259 (2014).
12. M. Lang, Ring conformations in bidisperse blends of ring polymers. *Macromolecules* **46**, 1158–1166 (2013).
13. J. Smrek, A. Y. Grosberg, Minimal surfaces on unconcatenated polymer rings in melt. *ACS Macro Lett.* **5**, 750–754 (2016).

14. S. P. Obukhov, Topologically induced glass transition in freely rotating rods. Jamming and rheology: Constrained dynamics on microscopic and macro-scopic scales. http://online.kitp.ucsb.edu/online/jamming/obukhov Accessed 5 October 2019.
15. D. Michieletto, M. S. Turner, A topologically driven glass in ring polymers. *Proc. Natl. Acad. Sci. U.S.A.* **113**, 5195–5200 (2016).
16. J. D. Halverson, J. Smrek, K. Kremer, A. Y. Grosberg, From a melt of rings to chromosome territories: The role of topological constraints in genome folding. *Rep. Prog. Phys.* **77**, 022601 (2014).
17. D. Marenduzzo, C. Micheletti, E. Orlandini, Biopolymer organization upon confinement. *J. Phys. Condens. Matter* **22**, 283102 (2010).
18. L. R. Gómez, N. A. García, T. Pöschel, Data from "Packing Structure of Semiflexible Rings." GitHub. https://github.com/garciana/PolymerRings. Deposited 26 January 2020.
19. K. Alim, E. Frey, Shapes of semiflexible polymer rings. *Phys. Rev. Lett.* **99**, 198102 (2007).
20. D. Jan Struik, *Lectures on Classical Differential Geometry* (Courier Corporation, 1961).
21. R. D. Kamien, The geometry of soft materials: A primer. *Rev. Mod. Phys.* **74**, 953–971 (2002).
22. M. Bernabei, P. Bacova, A. J. Moreno, A. Narros, C. N. Likos, Fluids of semiflexible ring polymers: Effective potentials and clustering. *Soft Matter* **9**, 1287–1300 (2013).
23. S. M. Rappaport, S. Medalion, Y. Rabin, Curvature distribution of worm-like chains in two and three dimensions. arXiv:0801.3183 (21 January 2008).
24. C. A. Weber *et al.*, Random bursts determine dynamics of active filaments. *Proc. Natl. Acad. Sci. U.S.A.* **112**, 10703–10707 (2015).
25. S. Jordens *et al.*, Adsorption at liquid interfaces induces amyloid fibril bending and ring formation. *ACS Nano* **8**, 11071–11079 (2014).

26. E. Orlandini, S. G. Whittington, Statistical topology of closed curves: Some applications in polymer physics. *Rev. Mod. Phys.* **79**, 611–642 (2007).
27. A. V. Vologodskii, V. V. Anshelevich, A. V. Lukashin, M. D. Frank-Kamenetskii, Statistical mechanics of supercoils and the torsional stiffness of the DNA double helix. *Nature* **280**, 294–298 (1979).
28. J. F. Marko, E. D. Siggia, Statistical mechanics of supercoiled DNA. *Phys. Rev. E* **52**, 2912–2938 (1995).
29. C. Micheletti, D. Marenduzzo, E. Orlandini, D. W. Summers, Knotting of random ring polymers in confined spaces. *J. Chem. Phys.* **124**, 064903 (2006).
30. K. Ostermeir, K. Alim, E. Frey, Confinement induces conformational transition of semiflexible polymer rings to figure eight form. *Soft Matter* **6**, 3467–3471 (2010).
31. R. Everaers *et al.*, Rheology and microscopic topology of entangled polymeric liquids. *Science* **303**, 823–826 (2004).
32. J. D. Bernal, A geometrical approach to the structure of liquids. *Nature* **183**, 141–147 (1959).
33. A. Donev *et al.*, Improving the density of jammed disordered packings using ellipsoids. *Science* **303**, 990–993 (2004).
34. M. Neudecker, S. Ulrich, S. Herminghaus, M. Schröter, Jammed frictional tetrahedra are hyperstatic. *Phys. Rev. Lett.* **111**, 028001 (2013).
35. S. Torquato, Y. Jiao, Dense packings of the Platonic and Archimedean solids. *Nature* **460**, 876–879 (2009).
36. L.-N. Zou, X. Cheng, M. L. Rivers, H. M. Jaeger, S. R. Nagel, The packing of granular polymer chains. *Science* **326**, 408–410 (2009).